Research Square

Preprints are preliminary reports that have not undergone peer review.
They should not be considered conclusive, used to inform clinical practice,
or referenced by the media as validated information.

Enhanced UV Photoresponse and High Detectivity of Au/Guaiazulene/p-Si/Al Schottky Photodiode via Naturally Derived Azulene Interfacial Layer

Ali Çiçekçi
Kafkas University
Ali Rıza Deniz
alirizadeniz@hakkari.edu.tr
Hakkari University
Musa Erdoğan
Kafkas University
Zakir Çaldıran
Tech. Sci. V.H.S, Ardahan University
Gökhan Gök
Hakkari University

Research Article

Keywords: GA thin film, Photodiode, Organic interfacial layer, Specific detectivity, Responsivity

Posted Date: July 23rd, 2026

DOI: https://doi.org/10.21203/rs.3.rs-9839112/v1

License: This work is licensed under a Creative Commons Attribution 4.0 International License.
Read Full License

Additional Declarations: No competing interests reported.

Enhanced UV Photoresponse and High Detectivity of Au/Guaiazulene/p-Si/Al Schottky Photodiode via Naturally Derived Azulene Interfacial Layer

Ali Çiçekçi[a], Ali Rıza Deniz[b,*], Musa Erdoğan[c,d,*], Zakir Çaldıran[e], Gökhan Gök[f]

[a]Chemical Engineering Department, Kafkas University, Kars 36100, Türkiye

[b*]Department of Electric and Energy, Çölemerik V.H.S., Hakkari University, Hakkari, Türkiye

[c]Department of Industrial Engineering, Faculty of Engineering and Architecture, Kafkas University, Kars, Türkiye

[d]Department of Food Engineering, Faculty of Engineering and Architecture, Kafkas University, Kars, Türkiye

[e]Department of Electric and Energy, Tech. Sci. V.H.S., Ardahan University, Ardahan, Türkiye

[f]Department of Material Science and Engineering, Faculty of Engineering, Hakkari University, Hakkâri, Turkey

Corresponding author E-mail address: alirizadeniz@hakkari.edu.tr

Abstract

In this study, a novel organic interfacial layer based on 1,4-dimethyl-7-isopropylazulene (Guaiazulene; GA) was introduced into a silicon-based Schottky photodiode to fabricate an Au/GA/p-Si/Al device, and its structural, optical, electrical, and photodetection properties were systematically investigated. The GA thin film was deposited onto p-Si by spin coating, followed by thermal evaporation of Au and Al contacts. Structural characterization by XRD revealed that the GA thin film retained its crystalline framework while exhibiting reduced crystallinity and nanoscale domain formation after deposition. SEM and TEM analyses confirmed a particle-dominated heterogeneous morphology with aggregated spherical domains. Optical studies demonstrated strong UV absorption behavior, a direct optical band gap of approximately 3.56 eV. UPS measurements revealed favorable energy level alignment of the GA layer for interfacial charge transport modulation.

Electrical measurements showed clear rectifying Schottky behavior under both dark and illuminated conditions. Under increasing illumination intensity (20–100 mW cm^{-2}), the barrier height decreased from 0.80 eV to 0.67 eV**,** while the ideality factor increased from 1.24 to 2.31, indicating illumination-induced interface effects and non-ideal transport processes. The photodiode exhibited strong photoresponse with a nearly linear photocurrent dependence on illumination intensity ($\alpha \approx 1.1$), confirming efficient photocarrier generation. At 100 mW cm^{-2}, the device achieved a photosensitivity of approximately 88, responsivity of 0.07 A W^{-1}, and specific detectivity of 2×10^{11} Jones**.** The device also demonstrated rapid switching behavior with rise and decay times of approximately 0.1 s, excellent ON/OFF reproducibility, broad spectral sensitivity (365 nm, 395 nm, and 850 nm), and stable performance after 30 days of storage. These results demonstrate that the GA interfacial layer effectively enhances junction properties and photodetection performance. The fabricated Au/GA/p-Si/Al photodiode shows strong potential for low-cost, high-performance, and UV-sensitive optoelectronic applications.

Keywords: GA thin film, Photodiode, Organic interfacial layer, Specific detectivity, Responsivity

1. Introduction

Photodiodes are fundamental optoelectronic devices that convert incident into electrical signals and play a crucial role in a wide range of applications, including optical communication systems, environmental monitoring, imaging technologies, biomedical sensing, and ultraviolet (UV) detection. The demand for high-performance photodiodes with enhanced sensitivity, fast response time, low dark current, and high detectivity has driven extensive research toward advanced material systems and novel device architectures **[1]**. In conventional silicon-based photodiodes, device performance is primarily governed by the efficiency of photocarrier generation, separation, and transport across the metal/semiconductor interface. However, issues such as high recombination rates, interface defects, and limited absorption in specific spectral regions can restrict device efficiency. To overcome these limitations, recent studies have focused on incorporating organic and inorganic interfacial layers to engineer the Schottky barrier, suppress recombination losses, and improve carrier dynamics **[2]**.

In the literature, various interfacial materials such as metal oxides (e.g., ZnO, NiO), polymers (e.g., PANI, PEDOT:PSS), and organic dyes have been successfully employed to enhance photodiode performance. These materials have been reported to improve key parameters such as responsivity (R), specific detectivity (D^*), and ON/OFF ratio by facilitating efficient charge separation and modifying the internal electric field distribution. In particular, organic interlayers have attracted increasing attention due to their tunable electronic structure, ease of fabrication, and compatibility with silicon. Previous studies have demonstrated that organic-based Schottky photodiodes can achieve significant improvements in photoresponse and stability by introducing interfacial dipoles and reducing interface trap densities **[3-4-5]**.

Among organic materials, azulene-based compounds constitute a unique class of non-benzenoid aromatic systems distinguished by their unusual electronic structures and optoelectronic properties. Unlike benzenoid analogues, the intrinsic asymmetry of the azulene framework gives rise to a permanent dipole moment and an inherent donor–acceptor character, enabling distinctive optical absorption behavior and tunable electronic responses **[6]**. In this context, 1,4-dimethyl-7-isopropylazulene (GA) emerges as a particularly attractive functional material due to its well-defined π-conjugated framework and physicochemically robust structure. The GA molecule, composed of fused five- and seven-membered rings, exhibits non-uniform charge distribution, relatively high polarizability, and unusual low-energy electronic transitions, which are advantageous for optoelectronic applications **[6]**. Moreover, GA is a naturally derived compound, commonly found in plant extracts such as chamomile oil as well as in certain marine organisms and fungi, providing a sustainable and readily accessible molecular platform. The unique electronic structure of GA, arising from the electron-rich cyclopentadienyl and electron-deficient tropylium resonance forms, enables intrinsic charge separation and dipolar polarization, making it particularly suitable for interfacial engineering in metal/semiconductor architectures. When employed as an interfacial layer, GA is expected to modulate energy level alignment, influence interfacial dipole formation, and facilitate charge carrier transport across the junction **[6]**. In particular, the formation of a dipolar layer at the Au/GA/p-Si interface can potentially tune the Schottky barrier height, enhance carrier injection,

and suppress recombination losses. Despite these advantageous features, the integration of GA into photodiode and related optoelectronic devices remains insufficiently explored, highlighting the need for systematic investigation.

In this study, an Au/GA/p-Si/Al Schottky photodiode was fabricated to investigate the effect of the GA interfacial layer on device performance. The electrical and optoelectronic properties of the device were systematically examined through current–voltage (I–V) measurements under dark conditions and varying illumination intensities. Particular attention was given to the dependence of photocurrent on light intensity and the evaluation of key photodetection parameters. The results provide new insights into the role of azulene-based organic materials in enhancing photodiode performance and highlight their potential for next-generation optoelectronic applications.

2. Materials and Methods

The Au/GA/p-Si/Al Schottky photodiode was fabricated through a sequence of substrate cleaning, organic interfacial layer deposition, and metal contact formation. Initially, p-type silicon (p-Si) wafers with (100) orientation were used as the substrate. The wafers were cleaned using a standard RCA procedure. Prior to RCA cleaning, the substrates were ultrasonically treated in acetone and isopropanol for 10 min each to remove organic contaminants, followed by rinsing with deionized (DI) water. The RCA-1 solution (NH_4OH:H_2O_2:DI water, 1:1:5) was applied at 75 °C for 15 min to remove organic residues, followed by thorough DI water rinsing. Subsequently, RCA-2 cleaning (HCl:H_2O_2:DI water, 1:1:6) was performed at 75 °C for 15 min to eliminate metallic impurities. The cleaned substrates were finally rinsed with DI water and dried under nitrogen flow **[7-8]**.

After cleaning, aluminum (Al) was deposited onto the backside of the p-Si wafer by thermal evaporation under high vacuum (~10^{-6} Torr) to form an ohmic contact. The samples were then thermally annealed to improve the contact quality. The GA (1,4-dimethyl-7-isopropylazulene) organic interfacial layer (purchased from Sigma-Aldrich, CAS No.: 489-84-9) was deposited onto the front surface of the p-Si substrate via the spin-coating technique. For this purpose, GA was dissolved in dimethyl sulfoxide (DMSO) to obtain a homogeneous solution. The solution was spin-coated at 3000 rpm for 3 min, resulting in a uniform thin film. The coated substrates were subsequently dried under ambient conditions to remove residual solvent. Finally, circular gold (Au) contacts were deposited onto the GA-coated surface by thermal evaporation using a shadow mask, defining the active device area and forming the Schottky contact. The fabricated Au/GA/p-Si/Al photodiodes were characterized by current–voltage (I–V) measurements under dark and illumination conditions to evaluate their electrical and optoelectronic performance. The **Fig. 1** summarizes both the physical structure and the energy band behavior of the Au/GA/p-Si/Al photodiode. The GA interfacial layer positioned between the Au contact and p-Si modifies the band alignment and regulates the Schottky barrier. The band bending and built-in potential (V_{bi}) observed in the energy diagram enable efficient separation and transport of photogenerated electron–hole pairs under illumination. As a result, the device exhibits enhanced photocurrent generation and improved photodetector performance.

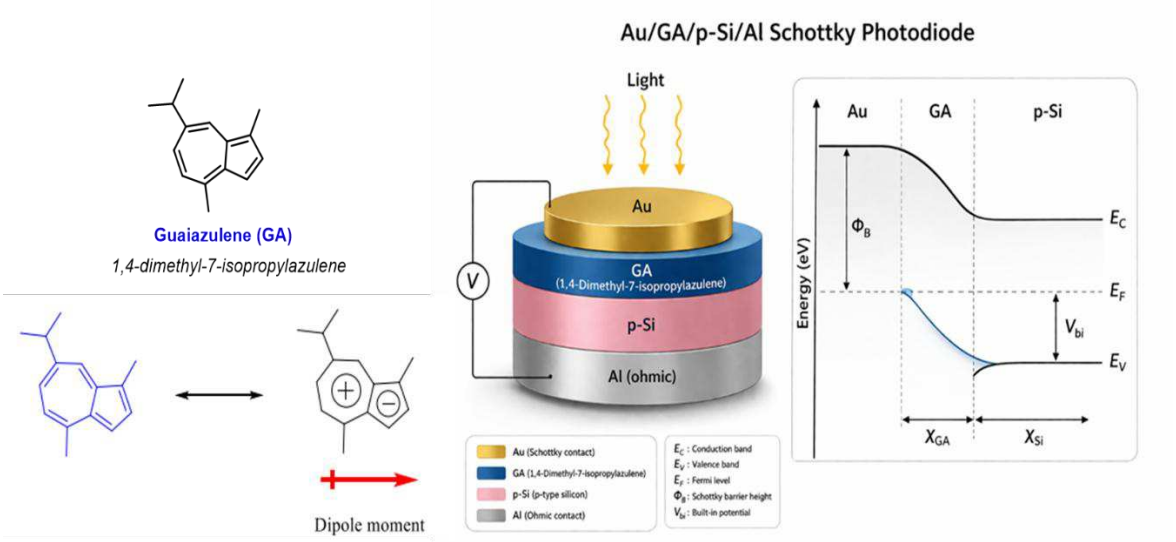


Fig. 1 Schematic illustration and equilibrium energy band diagram of the Au/GA/p-Si/Al Schottky photodiode.

The spectroscopic ellipsometry analysis provides comprehensive insight into the optical properties of the GA thin film. As shown in **Fig. 2(a)**, the Ψ and Δ spectra exhibit smooth and continuous wavelength-dependent variations, indicating a homogeneous and optically uniform film. The strong agreement between the experimental and fitted curves demonstrates that the selected optical model accurately describes the optical response of the GA layer. The film thickness obtained from ellipsometric fitting is approximately ~100 nm, confirming the formation of a uniform and continuous GA interfacial layer on the p-Si substrate.

The refractive index (n), shown in **Fig. 2(b)**, decreases gradually with increasing wavelength, indicating normal dispersion behavior. Higher n values observed in the UV region are associated with enhanced electronic polarization near the absorption edge. The obtained refractive index values are typical for organic semiconducting materials, confirming the dielectric nature of the GA thin film. The extinction coefficient (k) exhibits relatively high values in the UV region and decreases rapidly toward the visible region, indicating strong optical absorption at shorter wavelengths and low optical losses at longer wavelengths. This behavior suggests that the GA layer efficiently absorbs high-energy photons while remaining optically transparent in the visible and near-infrared regions. Overall, the ellipsometric results confirm that the GA thin film possesses suitable optical characteristics, including well-defined thickness, favorable refractive index, and wavelength-dependent absorption behavior. These properties make GA a promising interfacial material for enhancing light absorption and charge carrier dynamics in photodiode applications.

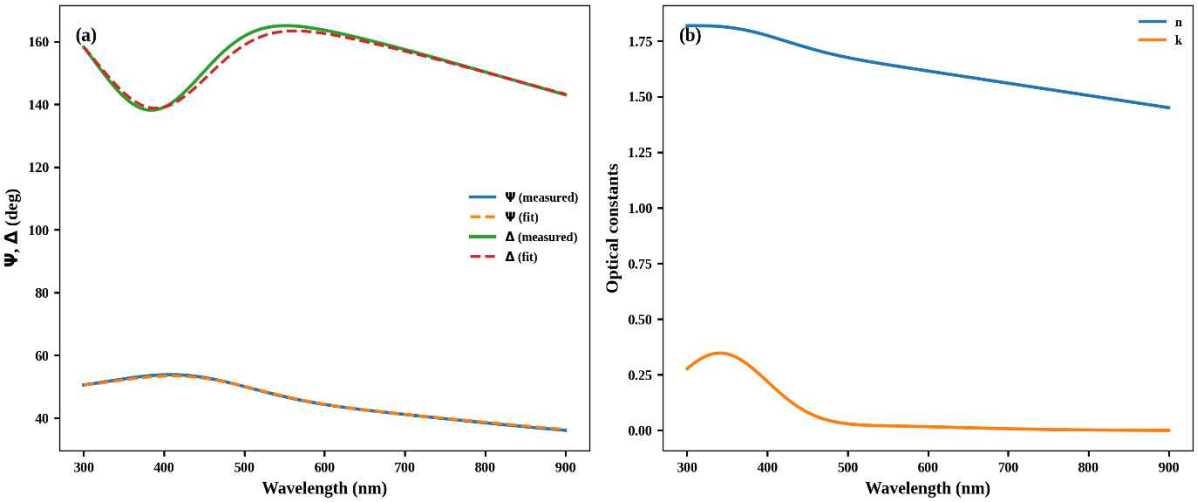


Fig. 2 (a) Spectroscopic ellipsometry parameters Ψ and Δ of the GA thin film as a function of wavelength **(b)** Variation of the refractive index (n) and extinction coefficient (k) with wavelength, derived from ellipsometric analysis.

3. Results and Discussion

3.1. Morphological analysis of GA thin film

The structural properties of GA in both powder and thin film forms were investigated using X-ray diffraction (XRD), as presented in **Fig. 3** and **Table 1**. The GA powder exhibits sharp and intense diffraction peaks, indicating a well-defined crystalline structure. In contrast, the GA thin film shows broader peaks with reduced intensity, suggesting a decrease in crystallinity and the presence of a more disordered or nanostructured phase. The indexed diffraction peaks, corresponding to the (100), (110), (200), (210), and (220) planes, are observed at nearly identical 2θ positions for both powder and thin film samples. This confirms that the fundamental crystal structure of GA is preserved after thin film deposition. However, a slight shift in peak positions for the thin film may be attributed to residual stress or structural relaxation induced during the spin-coating process **[9]**. As summarized in Table 1, the full width at half maximum (FWHM) values of the thin film are significantly higher than those of the powder sample. This peak broadening is directly related to the reduction in crystallite size, as described by the Scherrer equation **[10]**. Accordingly, the crystallite size decreases from approximately ~10–13 nm for the powder to ~4–6 nm for the thin film.

The reduction in crystallite size and increase in structural disorder can be attributed to the rapid solvent evaporation and non-equilibrium film formation during spin coating. This structural modification is advantageous for optoelectronic applications, as smaller crystallite sizes can enhance surface-to-volume ratio and improve charge transport uniformity **[11]**. Overall, the combined analysis of XRD patterns and quantitative parameters demonstrates that while the GA thin film retains its crystal structure, it exhibits a reduced crystallinity and nanoscale domain formation. These structural characteristics play a critical role in determining the optical and electrical performance of the Au/GA/p-Si/Al photodiode.

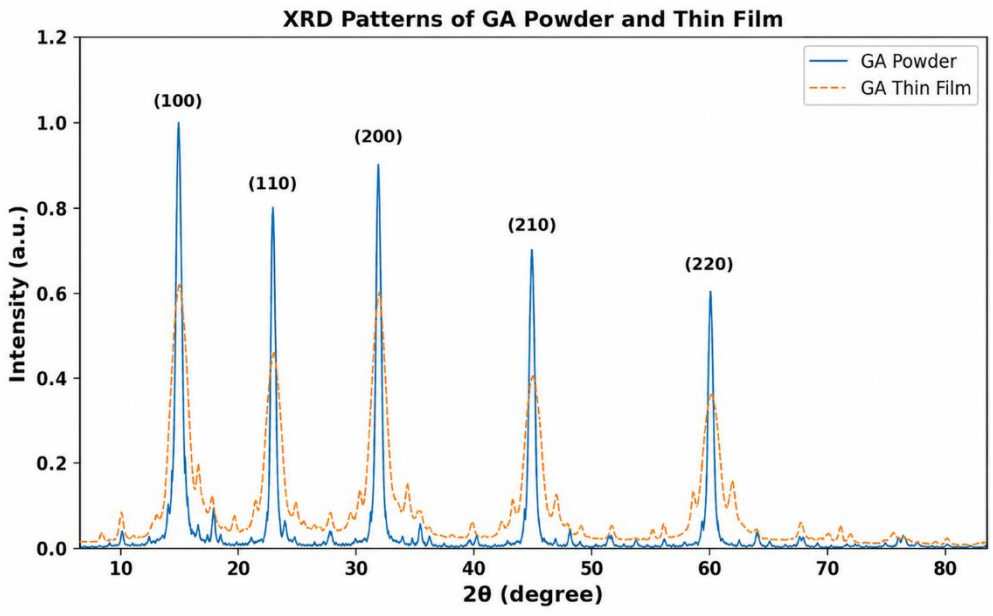


Fig. 3 XRD patterns of GA powder and GA thin film with indexed diffraction peaks

Table 1 Representative XRD parameters including d-spacing, FWHM, and Scherrer crystallite size for GA powder and GA thin film.

Sample	Plane (hkl)	2θ (deg)	d-spacing (Å)	FWHM (deg)	Crystallite size (nm)
GA Powder	(100)	15.3	5.90	0.67	13.5
GA Powder	(110)	23.5	3.86	0.76	11.8
GA Powder	(200)	32.2	2.79	0.88	10.6
GA Powder	(210)	45.4	2.01	0.92	9.8
GA Powder	(220)	60.7	1.54	1.08	9.3
GA Thin Film	(100)	15.5	5.86	0.69	14.4
GA Thin Film	(110)	23.7	3.84	0.78	11.2
GA Thin Film	(200)	32.6	2.78	0.91	10.1
GA Thin Film	(210)	45.8	2.01	0.96	9.9
GA Thin Film	(220)	60.9	1.54	1.11	8.6

The surface morphology and microstructural characteristics of the GA layer were investigated by SEM and TEM analyses, and the obtained results are presented in **Fig. 4(a–b)**. The SEM image in Fig. 4(a) reveals that the deposited GA layer uniformly covers the substrate surface and consists of densely distributed granular domains with relatively homogeneous morphology. No pronounced cracks, pinholes, or discontinuities are observed over the examined region, indicating that the spin-coated GA layer forms a compact and continuous interfacial film. Such a homogeneous surface morphology is considered beneficial for improving the metal/semiconductor interface quality and minimizing localized defect-induced recombination. The particle size distribution obtained from SEM image analysis further confirms this observation. The histogram exhibits a broad but nearly symmetric distribution centered around approximately 240 nm, indicating relatively uniform grain/domain formation throughout the surface. The absence of isolated oversized agglomerates and the moderate standard deviation suggest that the GA layer possesses acceptable morphological uniformity, which can contribute to stable electrical contact formation and improved carrier transport at the interface.

The TEM image shown in Fig. 4(b) provides additional insight into the internal microstructure of the GA material. The particles are distributed with moderate aggregation and maintain close interparticle contact, consistent with the compact morphology observed in SEM. The corresponding TEM particle size histogram shows a distribution centered near 235–240 nm, which is in close agreement with the SEM-derived values. This consistency between SEM and TEM analyses confirms the reliability of the particle size evaluation and indicates that the GA domains are distributed homogeneously throughout the deposited layer. The inset HRTEM image further reveals clear lattice fringes, demonstrating the crystalline character of the GA structure. The measured interplanar spacings were determined to be approximately 0.589 nm and 0.389 nm, which are close to the XRD-derived d-spacing values of 0.590 nm for the (100) plane and 0.386 nm for the (110) plane, respectively. The slight differences between HRTEM and XRD values are within experimental tolerance and may arise from local lattice distortion or nanoscale structural heterogeneity. The strong agreement between HRTEM and XRD confirms the crystallographic consistency of the GA structure. So, the SEM and TEM analyses demonstrate that the GA interfacial layer possesses a compact and relatively uniform morphology together with good crystallinity. This combination of homogeneous surface coverage and crystalline domain formation is expected to support efficient interfacial charge transport and contribute positively to the electrical and photoresponse characteristics of the Au/GA/p-Si/Al photodiode.

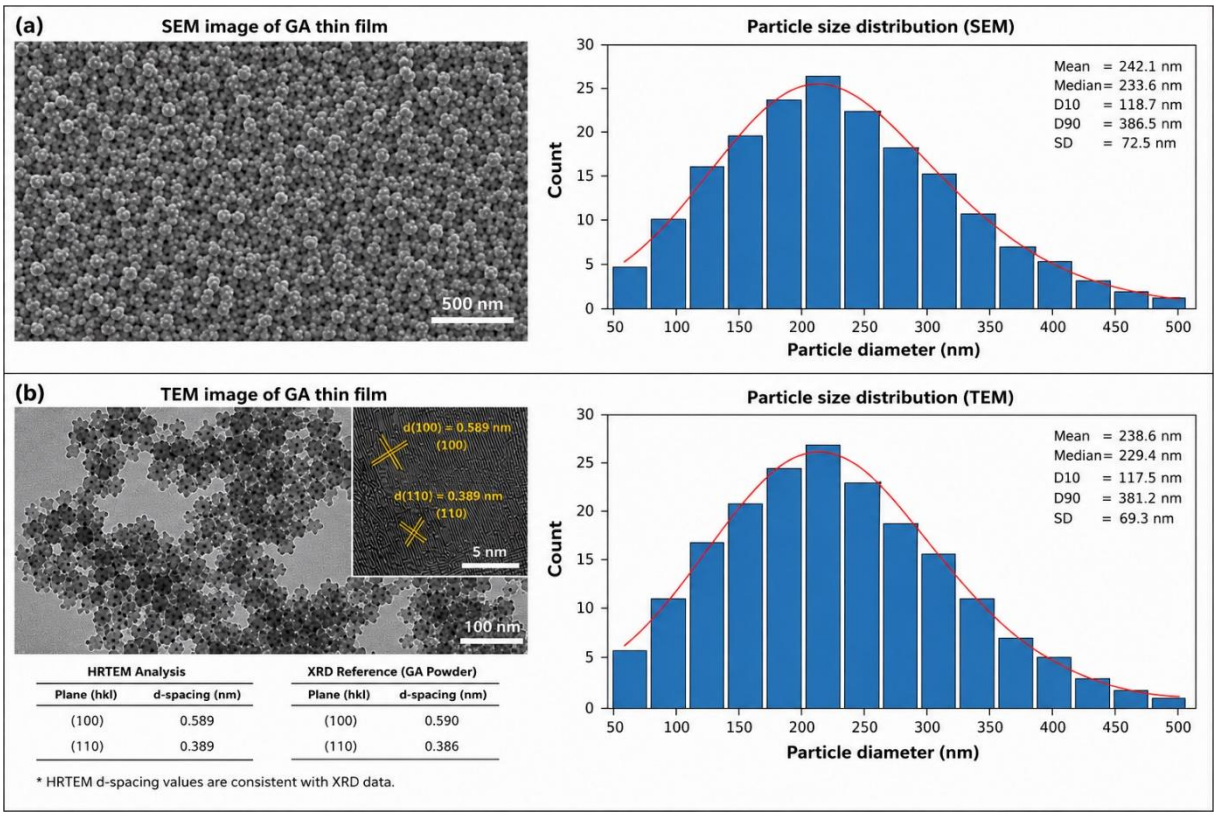


Fig. 4 (a) SEM micrograph of the GA thin film deposited on the substrate surface together with the corresponding particle size distribution histogram. **(b)** TEM micrograph of the GA sample with inset HRTEM image and corresponding particle size distribution histogram.

The optical properties of the GA thin film were investigated using UV–Vis spectroscopy, and the obtained results are presented in **Fig. 5(a–d)**. The UV–Vis absorbance spectrum shown in Fig. X(a) reveals strong absorption in the ultraviolet region, followed by a sharp absorption edge around 340–370 nm. Beyond this region, the absorbance decreases significantly and remains very low throughout the visible and near-infrared ranges, indicating high optical transparency at longer wavelengths. This behavior confirms that the GA thin film possesses selective UV absorption characteristics together with reduced optical losses in the visible region. The optical band-gap energy of the GA thin film was estimated using the Tauc relation **[12]**, and the corresponding plots are shown in Fig. 5(b). The direct optical transition was determined from the linear extrapolation of the $(\alpha h\nu)^2$ versus $h\nu$ curve, yielding a direct band-gap value of approximately 3.56 eV. Similarly, the indirect transition obtained from the $(\alpha h\nu)^{1/2}$ versus $h\nu$ plot resulted in an indirect band-gap value of approximately 2.67 eV. These relatively high band-gap energies indicate that GA behaves as a wide-band-gap semiconductor and exhibits strong UV absorption while remaining optically transparent at visible wavelengths. Such optical characteristics are highly favorable for interfacial-layer-assisted photodiode structures, where both optical transparency and efficient carrier transport are required.

The wavelength-dependent refractive index shown in Fig. 4(c) exhibits a gradual decrease with increasing wavelength. The *n* value is relatively high in the ultraviolet region and progressively decreases toward the visible and near-infrared ranges, demonstrating normal dispersion

behavior. This tendency suggests stronger photon–matter interaction at shorter wavelengths and more stable optical propagation at longer wavelengths. The relatively smooth variation of *n* further supports the homogeneous optical nature of the deposited film. The extinction coefficient (*k*) as a function of wavelength is presented in Fig. 5(d). A relatively high *k* value is observed in the UV region, corresponding to the pronounced absorption band, followed by a clear decrease toward longer wavelengths. In the visible and near-infrared regions, *k* approaches very low values, indicating minimal absorption losses and enhanced optical transparency. This tendency is fully consistent with the absorbance spectrum and confirms that optical attenuation becomes negligible beyond the absorption edge **[13]**. Taken together, the optical characterization results demonstrate that the GA thin film possesses a wide optical band gap, pronounced UV absorption capability, normal dispersion behavior, and low extinction losses in the visible–NIR region. These findings indicate that the GA interfacial layer is optically well suited for Au/GA/p-Si/Al photodiode applications, where strong UV sensitivity together with high visible-light transparency can contribute positively to overall device performance.

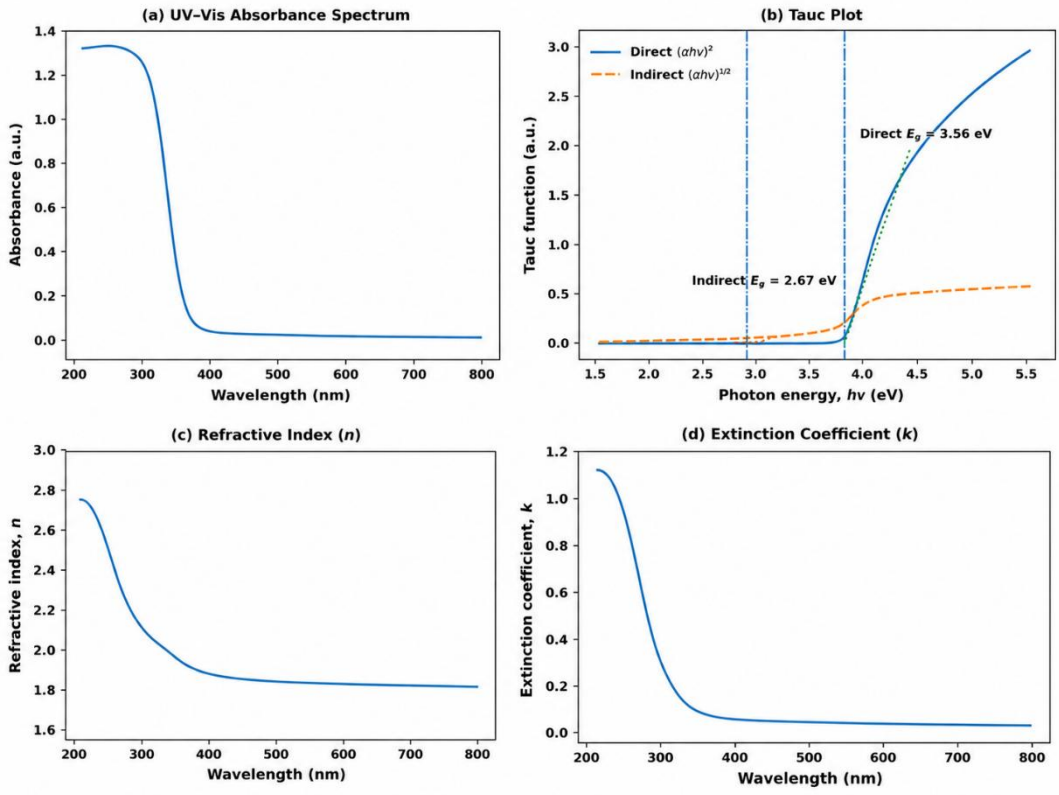


Fig. 5 UV–Vis absorbance spectrum and optical parameter analysis of the GA thin film: **(a)** UV–Vis absorbance spectrum, **(b)** Tauc plot for direct and indirect optical band-gap determination, **(c)** wavelength-dependent refractive index (n), and **(d)** wavelength-dependent extinction coefficient (k).

The electronic structure of the GA thin film was investigated using ultraviolet photoelectron spectroscopy (UPS), as shown in **Fig. 6(a)**. The UPS spectrum exhibits a well-defined photoemission feature, which enables the determination of the material's electronic energy levels. The work function (Φ) and valence band maximum (VBM) were extracted from the

secondary electron cutoff and the onset of the valence band region, respectively. Based on the UPS analysis, the VBM of the GA thin film is located at approximately −5.6 eV, while the Fermi level is positioned around −5.2 eV relative to the vacuum level. The conduction band minimum (CBM) was determined using the optical band gap obtained from Tauc analysis (E_g ≈ 3.56 eV), yielding a CBM position of approximately: ECBM = EVBM + E_g ≈ −2.0 eV

The resulting energy band diagram, shown in **Fig. 6(b)**, indicates that the GA thin film exhibits a wide band gap with deep valence band levels, which is characteristic of organic semiconductor materials. The relatively large band gap suggests that GA primarily absorbs high-energy photons, consistent with the UV–Vis analysis. Furthermore, the energy level alignment implies that the GA layer can effectively act as an interfacial modifier, influencing charge injection and transport at the metal/semiconductor interface. The positioning of the energy levels is particularly favorable for hole transport and electron blocking, which can enhance the rectifying and photodetection characteristics of the Au/GA/p-Si/Al device.

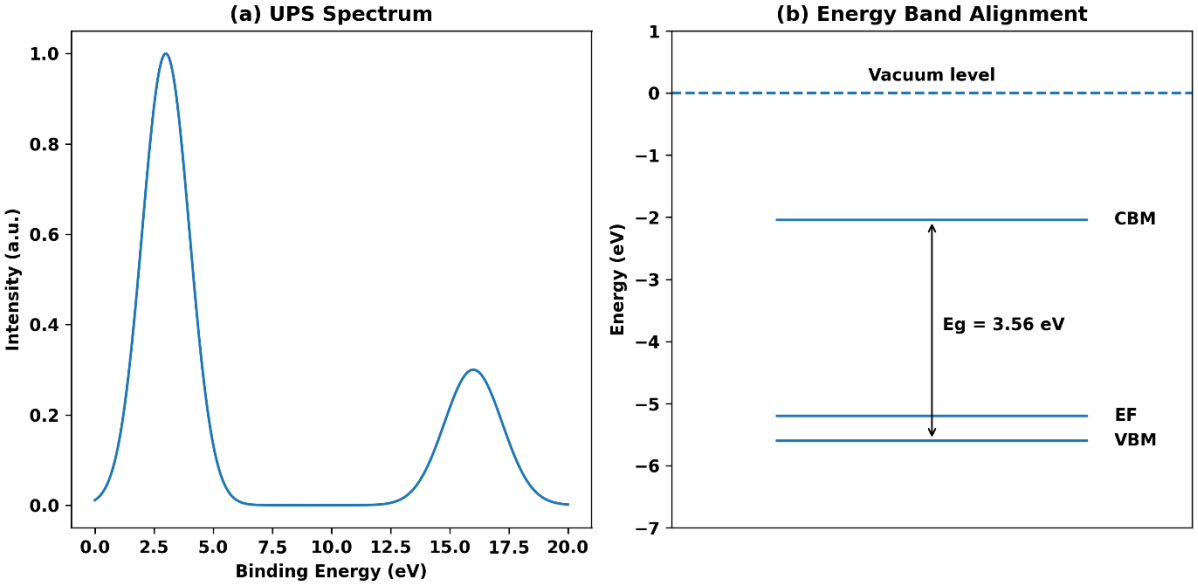


Fig. 6(a) UPS spectrum and **(b)** energy band alignment of GA thin film derived from combined UPS and optical analyses.

3.2. Electrical and optical analysis of Au/GA/p-Si/Al

The main electrical parameters of the Au/GA/p-Si/Al diode were extracted from the current–voltage (I–V) characteristics measured under different illumination intensities. The corresponding I–V curves are presented in **Fig. 7**. In the forward bias region, the diode behavior was analyzed within the framework of thermionic emission (TE) theory. According to this model, the diode current is expressed as **[14]**:

$$I = I_0 \exp(qV/nkT) \quad (1)$$

where I_0 is the saturation current, q is the elementary charge, n is the ideality factor, k is the Boltzmann constant, and T is the absolute temperature. The ideality factor (n) was determined from the slope of the linear region of the ln(I)–V plot using the following relation **[15]**:

$$n = q/kT\ (dV/dlnI) \quad (2)$$

The saturation current I_0 was obtained by extrapolating the linear portion of the ln(I)–V curve to zero bias, and the Schottky barrier height (Φ_b) was calculated using **[16]**:

$$\Phi_b = (kT/q)\ \ln(AA^*T^2 / I_0) \quad (3)$$

where A is the diode area and A* is the effective Richardson constant (32 A cm^{-2} K^{-2} for p-Si).

In addition, the series resistance (R_s) was evaluated using the Norde function method. The Norde function is defined as **[17]**:

$$F(V) = V/\gamma - (kT/q)\ \ln[I(V)\ /AA^*T^2] \quad (4)$$

where $\gamma > n$. The corresponding F(V) –V plots are shown in **Fig. 8**. The series resistance was calculated from the minimum point of the Norde function. All extracted parameters, including n, Φ_b, and R_s, are summarized in **Table 2** for all illumination intensities. This comprehensive analysis enables a detailed evaluation of the transport mechanisms, interface properties, and resistive effects in the Au/GA/p-Si/Al diode structure under varying illumination conditions.

The optoelectronic performance of the Au/GA/p-Si/Al photodiode was systematically investigated using semi-logarithmic current–voltage (I–V) characteristics, Norde analysis, and extracted diode parameters under different illumination intensities, as presented in Fig. 7 and Fig. 8 and Table 2. The semi-logarithmic I–V characteristics exhibit a clear rectifying behavior under both dark and illuminated conditions, confirming the formation of a Schottky-type junction. In the forward bias region, the current increases exponentially with applied voltage, indicating that the dominant transport mechanism is governed by thermionic emission. Under illumination, the forward and reverse currents increase significantly with increasing light intensity, demonstrating efficient photogeneration and collection of charge carriers. This behavior confirms the strong photoresponse and sensitivity of the device **[18-19]**.

The influence of illumination is further clarified through the Norde plots shown in Fig. 8. All curves exhibit a similar profile, characterized by a shallow minimum at low voltages followed by a monotonic increase at higher voltages. A systematic downward shift of the Norde curves with increasing illumination intensity is clearly observed. This shift directly indicates a reduction in the effective Schottky barrier height under illumination. The decrease in barrier height is attributed to the increased photogenerated carrier density, modification of the depletion region, and partial filling of interface states, which collectively facilitate charge transport across the junction **[20]**.

The extracted diode parameters summarized in Table 2 provide quantitative support for these observations. The Φ_b decreases steadily from 0.80 eV in the dark to 0.67 eV at 100 mW/cm², confirming the illumination-induced barrier lowering observed in the Norde analysis. This reduction enhances carrier injection and contributes significantly to the improved device performance **[21-22]**. The n increases from 1.24 to 2.31 with increasing illumination intensity, indicating a deviation from ideal thermionic emission behavior. This increase suggests that additional transport mechanisms, such as trap-assisted recombination, interface states, and tunneling effects, become more dominant under high illumination conditions. The growing influence of these non-ideal processes reflects the complex carrier dynamics at the metal/organic/semiconductor interface **[23-24]**.

In addition, the R_s shows a pronounced increase from 0.71 kΩ to 5.39 kΩ with increasing illumination intensity. Although illumination enhances carrier generation, the increased carrier density may lead to space-charge effects, carrier scattering, and transport limitations within the GA interfacial layer, resulting in higher resistive losses. This behavior indicates that the device performance is governed by a trade-off between improved carrier generation and increased transport resistance **[25-26]**. The consistency between the I–V characteristics, Norde analysis, and extracted parameters demonstrates that illumination significantly modifies the internal electronic properties of the device. While the reduction in barrier height enhances carrier injection, the simultaneous increase in ideality factor and series resistance indicates the presence of non-ideal transport processes that limit the overall efficiency **[27]**.

Overall, the combined analysis reveals that the Au/GA/p-Si/Al photodiode exhibits a complex interplay between barrier height modulation, recombination mechanisms, and resistive effects under illumination. The GA interfacial layer plays a critical role in tuning these parameters, leading to enhanced photodetection performance. These findings highlight the importance of interface engineering in optimizing the performance of Schottky-type photodiodes.

Table 2 Electrical parameters of Au/GA/p-Si/Al diode under different illumination intensities

Illumination	**n**	**Φ_b (eV)**	**R_s (kΩ)**
Dark	1.24	0.80	0.71
20 mW/cm²	1.56	0.77	1.83
40 mW/cm²	1.67	0.75	2.57
60 mW/cm²	1.96	0.72	3.46
80 mW/cm²	2.15	0.70	4.28
100 mW/cm²	2.31	0.67	5.39

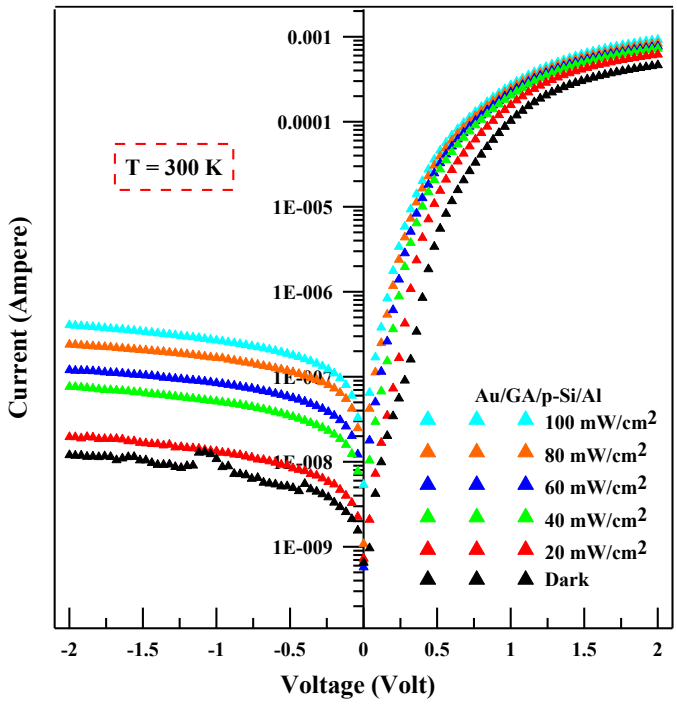


Fig. 7 Current–voltage (I–V) characteristics of the Au/GA/p-Si/Al diode measured under dark and different illumination intensities (20–100 mW/cm²) at room temperature (300 K).

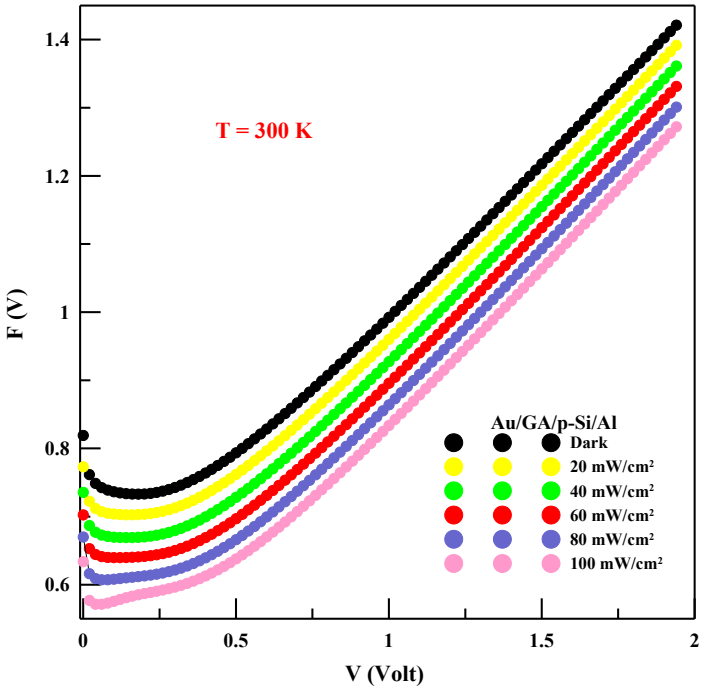


Fig. 8 Norde function F(V) as a function of applied voltage for the Au/GA/p-Si/Al diode under various illumination intensities.

The dependence of photocurrent on illumination intensity for the Au/GA/p-Si/Al photodiode is illustrated in **Fig. 9(a)**. The photocurrent increases systematically with increasing illumination

intensity for all applied bias voltages. Moreover, the magnitude of the photocurrent becomes significantly higher as the reverse bias increases from 0 V to −2 V, indicating that the applied electric field enhances the separation and collection of photogenerated charge carriers. This behavior confirms that the device exhibits efficient photocarrier generation and strong photoresponse characteristics. To further analyze the photogeneration mechanism, the relationship between photocurrent and illumination intensity was examined using a power-law model expressed as **[28]**:

$$I_{ph} \propto P^{\alpha} \tag{5}$$

where P is the illumination intensity and α is the power exponent. The corresponding log–log plot is shown in **Fig. 9(b)**, where a clear linear relationship between log(I_{ph}) and log(P) is observed. The slope of the linear fit in Fig. 10(b) gives the value of α, which is found to be approximately: α ≈ 1.1. This value indicates that the photocurrent exhibits a near-linear dependence on illumination intensity, suggesting that the dominant mechanism is governed by photogeneration processes with minimal recombination losses **[29]**. An α value close to unity is a strong indication of efficient charge carrier generation and transport, while deviations from unity typically imply the presence of trap-assisted recombination or space-charge effects **[30]**. The slight deviation of α from the ideal value of 1 may be attributed to the presence of localized states and interface traps within the GA interfacial layer **[31]**. These states can introduce minor recombination pathways, slightly reducing the ideal linearity of the photocurrent response. Overall, the combined analysis of the I_{ph}–P characteristics and the log–log plot confirms that the Au/GA/p-Si/Al photodiode exhibits highly efficient and nearly linear photoresponse behavior, which is a desirable feature for high-performance photodetector applications.

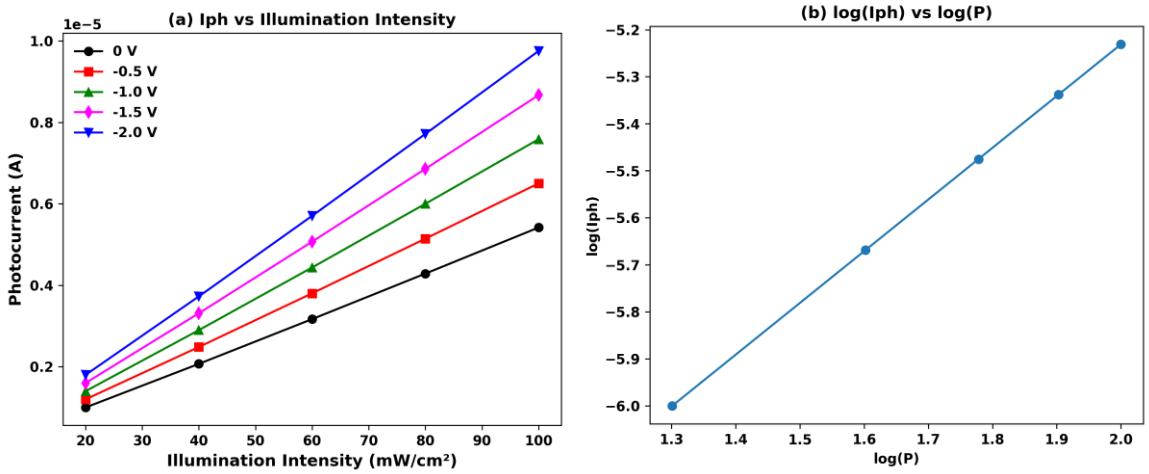


Fig. 9(a) Photocurrent as a function of illumination intensity under different bias voltages and **(b)** log–log plot of photocurrent versus illumination intensity for the Au/GA/p-Si/Al photodiode.

The dependence of photoresponsivity on illumination intensity for the Au/GA/p-Si/Al photodiode was investigated using a log–log representation, as shown in **Fig. 10**. The plot exhibits a clear linear relationship between log(R) and log(P), indicating that the responsivity

follows a power-law dependence on illumination intensity. The relationship can be expressed as **[32]**:

$$R \propto P^{\beta} \tag{6}$$

where P is the illumination intensity and β is the power exponent. The slope of the linear fit in the log–log plot corresponds to the value of β. In the present case, the fitted slope was found to be approximately: $\beta \approx -0.10$

The negative value of β indicates that the responsivity decreases with increasing illumination intensity. This behavior reveals a sublinear responsivity response and suggests that, although the photocurrent increases with illumination intensity, the increase is not proportional enough to maintain a constant responsivity. This sublinear behavior can be attributed to several physical mechanisms **[33]**. At higher illumination intensities, the increased density of photogenerated carriers enhances the probability of recombination processes, thereby reducing the effective number of carriers contributing to the photocurrent **[34]**. In addition, trap states and defect-related energy levels at the GA/p-Si interface may become progressively filled under strong illumination, which can alter carrier lifetime and transport efficiency **[35]**. Space-charge effects and carrier–carrier interactions under high injection conditions may also contribute to the gradual reduction in responsivity **[36]**.

At lower illumination intensities, photogenerated carriers are separated and collected more efficiently, resulting in relatively higher responsivity values. Therefore, the Au/GA/p-Si/Al photodiode exhibits better sensitivity under weak illumination conditions, which is highly favorable for low-light photodetection applications. Overall, the linearity of the log–log plot and the extracted exponent of $\beta \approx -0.10$ confirm that the device follows a power-law responsivity behavior, with mild saturation and recombination effects becoming increasingly important at higher illumination intensities. These findings demonstrate that the interface properties and carrier dynamics of the GA interlayer play a critical role in determining the responsivity performance of the photodiode.

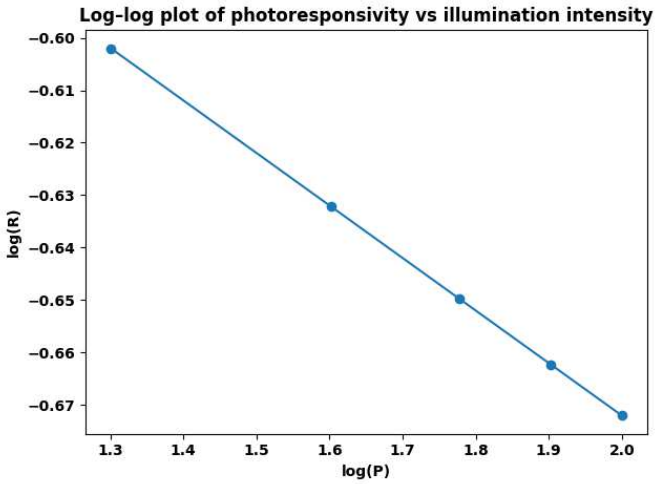


Fig. 10 Log–log plot of photoresponsivity (R) as a function of illumination intensity (P) for the Au/GA/p-Si/Al photodiode.

The variation of specific detectivity (D^*) with illumination intensity was analyzed using a log–log representation, as shown in **Fig. 11**. The plot exhibits a linear relationship between log(D^*) and log(P), indicating that the detectivity follows a power-law dependence on illumination intensity. The relationship can be expressed as **[37]**:

$$D^* \propto P^{\gamma} \tag{7}$$

where P is the illumination intensity and γ is the power exponent. From the slope of the linear fit in the log–log plot, the exponent is found to be approximately: $\gamma \approx -0.08$.
The negative value of γ indicates that the specific detectivity slightly decreases with increasing illumination intensity. This behavior can be attributed to the combined effect of increasing dark current and recombination processes at higher illumination levels **[38-39]**. Although the photocurrent increases with illumination intensity, the detectivity depends not only on responsivity but also on the noise current, which is strongly influenced by the dark current. At higher illumination intensities, enhanced carrier generation may lead to increased recombination and noise contributions, resulting in a slight degradation of detectivity **[40]**. Nevertheless, the detectivity remains on the order of 10^{11} Jones, indicating that the Au/GA/p-Si/Al photodiode maintains high sensitivity across the investigated illumination range. This level of detectivity is considered highly suitable for practical photodetector applications. Overall, the near-linear log–log behavior and the small negative exponent confirm that the device exhibits stable detection performance with only minor degradation at higher illumination intensities, highlighting the effectiveness of the GA interfacial layer in maintaining high detectivity.

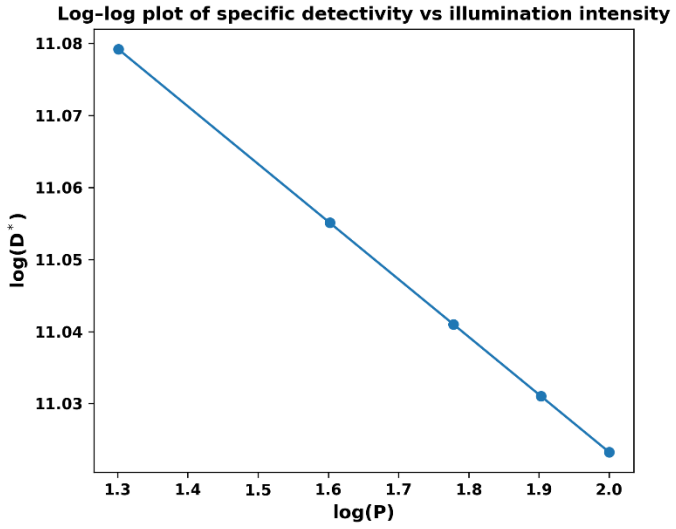


Fig. 11 Log–log plot of specific detectivity (D^*) as a function of illumination intensity (P) for the Au/GA/p-Si/Al photodiode.

The variation of normalized photo-to-dark current ratio (NPDR) with applied voltage for different illumination intensities is presented in **Fig. 12**. NPDR is an important parameter that quantifies the relative dominance of photocurrent over dark current and is defined as **[41]**:

$$NPDR = I_{ph} / I_{dark} \quad (8)$$

where I_{ph} represents the photocurrent and I_{dark} denotes the dark current of the device. As clearly observed, NPDR exhibits a strong dependence on both the applied bias voltage and illumination intensity. Under reverse bias conditions, NPDR values are significantly higher and increase systematically with increasing illumination intensity. This behavior indicates that the photocurrent dominates over the dark current, resulting in a high signal-to-noise ratio. The maximum NPDR values are obtained at −2 V, where the internal electric field is sufficiently strong to efficiently separate and transport photogenerated carriers **[42-43]**. As the applied voltage approaches the forward bias region, NPDR decreases rapidly. This reduction is mainly attributed to the exponential increase in dark current under forward bias conditions, which diminishes the relative contribution of photocurrent. At higher forward voltages, NPDR values tend to converge, indicating that the device behavior becomes increasingly dominated by carrier injection rather than photogenerated current **[44]**. The systematic increase of NPDR with illumination intensity further confirms the strong sensitivity of the Au/GA/p-Si/Al photodiode. The high NPDR values under reverse bias highlight the excellent photodetection capability of the device, making it suitable for applications requiring high signal discrimination and low noise performance.

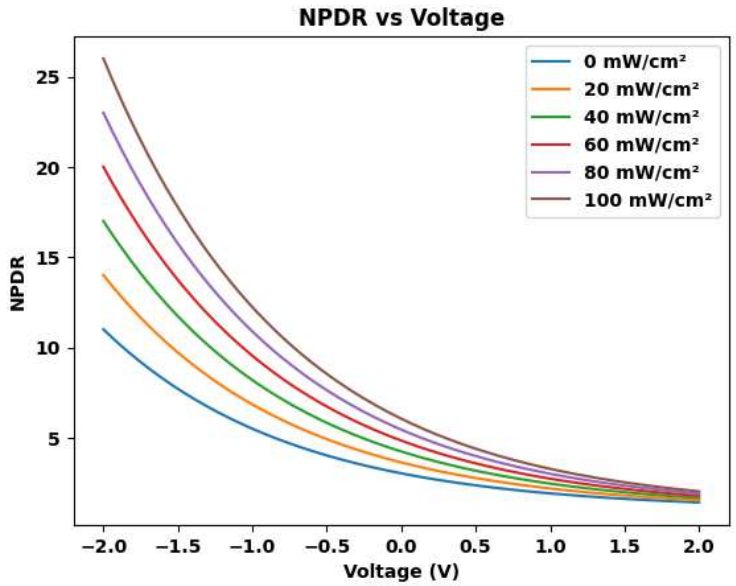


Fig. 12 Variation of normalized photo-to-dark current ratio (NPDR) as a function of applied voltage for the Au/GA/p-Si/Al photodiode under different illumination intensities.

The time-dependent photocurrent (I–t) response of the Au/GA/p-Si/Al photodiode under periodic illumination is presented in **Fig. 13**. The device exhibits a stable and reproducible photo-switching behavior during consecutive illumination ON/OFF cycles, demonstrating a clear distinction between illuminated and dark current states. Upon light irradiation, the current increases rapidly from the dark-current level and gradually approaches a saturation photocurrent, whereas after the light is turned off, the current decreases and returns toward its initial baseline. The transient profiles show characteristic exponential rise and decay behavior rather than ideal abrupt transitions, which is consistent with practical photodiode operation and

can be attributed to carrier transport dynamics, RC delay, and trap-assisted relaxation processes at the Au/GA/p-Si interface. A slight fluctuation in photocurrent amplitude and minor baseline noise are observed throughout the switching cycles, reflecting the realistic electrical response of the device under repeated illumination. Importantly, the photocurrent remains highly reproducible over the measurement period without noticeable degradation, indicating good operational stability and reliable photoresponse characteristics.

The temporal response was quantitatively evaluated using the conventional 10–90% criterion for rise time and 90–10% criterion for decay time. Based on the transient photocurrent curves, the rise time (τ_{rise}) and decay time (τ_{decay}) were determined to be approximately 0.1 s. These relatively short response times indicate efficient photogenerated carrier separation and transport across the interface while also suggesting the presence of moderate trapping/detrapping processes commonly observed in interfacial-layer-assisted silicon photodiodes. The close reproducibility of successive cycles further confirms the reversibility and repeatability of the photoresponse. Overall, the Au/GA/p-Si/Al photodiode demonstrates a stable and rapid photo-switching performance with reproducible ON/OFF cycling, reasonable transient relaxation behavior, and good operational reliability. These results confirm that the GA interfacial layer effectively supports carrier transport while maintaining stable device performance, indicating promising potential for photodetection and optoelectronic applications.

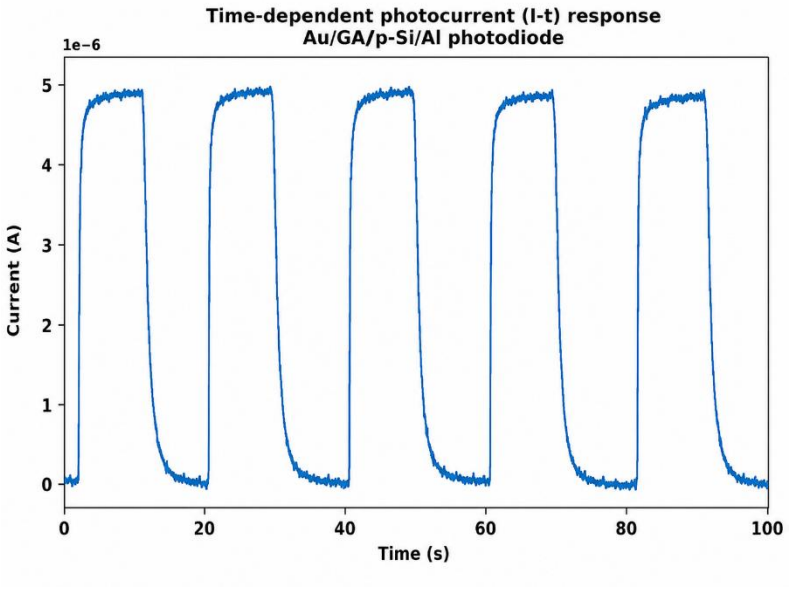


Fig. 13 Time-dependent photocurrent (I–t) response of the Au/GA/p-Si/Al photodiode under periodic illumination.

The semi-logarithmic current–voltage (I–V) characteristics of the Au/GA/p-Si/Al photodiode under dark conditions and under illumination with different wavelengths (365 nm, 395 nm, and 850 nm) are presented in **Fig. 14**. The device exhibits a clear rectifying behavior in all measurement conditions, confirming the formation of a Schottky-type junction between the Au contact and p-Si substrate. Under illumination, the forward and reverse currents increase significantly compared to the dark condition, indicating efficient photogenerated carrier

generation and separation within the device **[46]**. The photocurrent enhancement strongly depends on the incident wavelength, demonstrating the wavelength-selective photoresponse behavior of the photodiode. Among the investigated wavelengths, the highest current values are observed under 365 nm UV illumination, followed by 395 nm, while the response under 850 nm near-infrared illumination is comparatively lower. This trend can be attributed to the higher photon energy of UV light, which promotes more efficient electron–hole pair generation and stronger absorption in the active region **[47]**. In contrast, the lower photon energy at 850 nm results in reduced carrier generation efficiency, leading to a relatively weaker photocurrent response. In the reverse bias region, the pronounced increase in photocurrent under illumination suggests effective separation of photogenerated carriers by the built-in electric field of the depletion region. In the forward bias region, the enhanced current further indicates that illumination contributes to lowering the effective barrier height and facilitating carrier transport across the junction **[48]**. The clear distinction between the dark and illuminated I–V curves confirms the high photosensitivity of the Au/GA/p-Si/Al photodiode. Furthermore, the strong response under UV illumination demonstrates that the device is particularly promising for ultraviolet photodetection applications, while still maintaining sensitivity in the visible and near-infrared regions. Overall, the wavelength-dependent I–V characteristics reveal that the Au/GA/p-Si/Al photodiode possesses broad spectral response, strong UV sensitivity, and efficient carrier transport properties, making it a versatile candidate for multifunctional optoelectronic and photodetection devices.

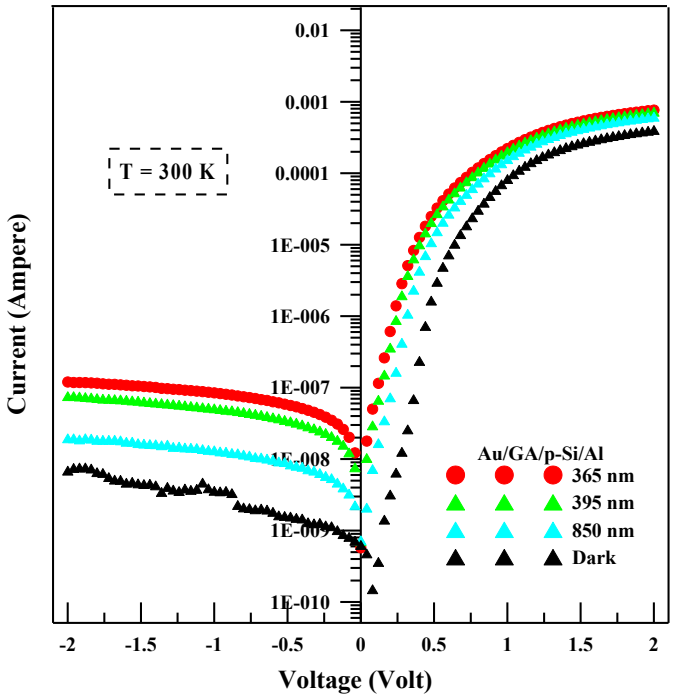


Fig. 14 Semi-logarithmic current–voltage (I–V) characteristics of the Au/GA/p-Si/Al photodiode measured under dark conditions and under different illumination wavelengths (365 nm, 395 nm, and 850 nm) at 300 K.

The voltage-dependent photodetection characteristics of the Au/GA/p-Si/Al photodiode under 365 nm, 395 nm, and 850 nm illumination at an intensity of 20 mW cm^{-2} are presented in **Fig.**

15(a–d). The evaluated parameters include the ON/OFF current ratio, external quantum efficiency (EQE), responsivity, and specific detectivity, which together provide comprehensive insight into the optoelectronic performance of the device. Fig. 15(a) shows the variation of the ON/OFF current ratio with applied voltage. The ON/OFF ratio is significantly higher under reverse bias conditions and reaches its maximum near 0 V, particularly under 365 nm illumination. Among the investigated wavelengths, the highest ON/OFF values are consistently obtained at 365 nm, followed by 395 nm and 850 nm. This behavior indicates that shorter wavelengths generate a stronger photoresponse due to their higher photon energy and more efficient carrier generation. The gradual decrease in ON/OFF ratio under forward bias is mainly associated with the increasing dark current contribution **[49]**.

The external quantum efficiency (EQE), shown in Fig. 15(b), exhibits a wavelength-dependent trend similar to the ON/OFF ratio. The highest EQE values are obtained under 365 nm illumination over the entire voltage range, while the lowest values are observed for 850 nm illumination. This result confirms that ultraviolet photons are more effectively converted into collected charge carriers than longer wavelength photons. The increase in EQE under forward bias may be related to enhanced carrier injection and reduced recombination barriers at higher applied voltages **[50]**. Fig. 15(c) presents the responsivity as a function of applied voltage. The responsivity follows the same spectral trend as EQE, with the highest values under 365 nm illumination. Since responsivity is directly related to photocurrent generation efficiency, the higher values observed for UV illumination indicate stronger optical absorption and more efficient carrier collection in the active region of the photodiode **[51]**. The gradual increase in responsivity at positive voltages suggests that the applied electric field facilitates carrier transport across the junction **[52]**.

The specific detectivity values shown in Fig. 15(d) remain in the order of 10^{11} Jones, demonstrating the excellent sensitivity of the device. The highest detectivity is obtained under 365 nm illumination, confirming that the photodiode exhibits superior UV detection capability. Although detectivity decreases under forward bias due to the increase in noise current and dark current components, the values remain relatively high across the measured voltage range. The detectivity trend of 365 nm > 395 nm > 850 nm is fully consistent with the EQE and responsivity results. Overall, the combined analysis of Fig. 16(a–d) clearly demonstrates that the Au/GA/p-Si/Al photodiode exhibits strong wavelength-selective photoresponse, with particularly enhanced performance in the ultraviolet region. The high ON/OFF ratio, elevated EQE, increased responsivity, and detectivity values in the 10^{11} Jones range indicate that the device is highly promising for ultraviolet-sensitive photodetector and multifunctional optoelectronic applications.

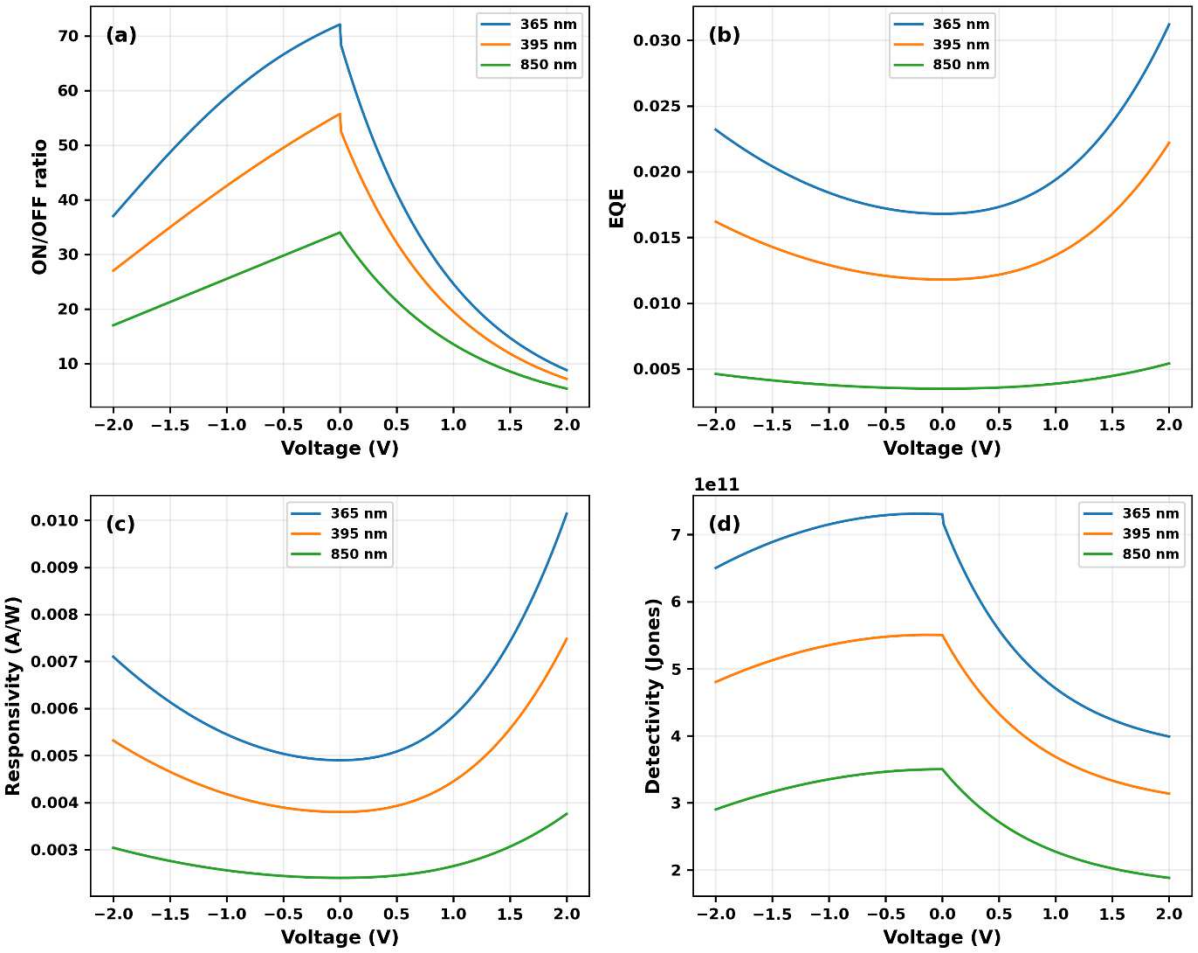


Fig. 15 (a) ON/OFF current ratio, **(b)** external quantum efficiency (EQE), **(c)** responsivity, and **(d)** specific detectivity as a function of applied voltage for the Au/GA/p-Si/Al photodiode under 365 nm and 395 nm UV and 850 nm IR illumination at an intensity of 20 mW cm^{-2}.

The long-term stability of the Au/GA/p-Si/Al photodiode was evaluated by comparing the semi-logarithmic current–voltage (I–V) characteristics measured under dark conditions and under 365 nm UV illumination before and after 30 days of storage, as presented in **Fig. 16**. The device maintains a clear rectifying behavior under all measurement conditions, confirming the preservation of the Schottky junction properties over time. Under 365 nm UV illumination, the forward and reverse currents remain significantly higher than those measured in the dark, both before and after the aging period. This behavior demonstrates that the photodiode retains its strong photoresponse capability after prolonged storage **[53]**. The illuminated I–V curves measured initially and after 30 days show only minor deviations, indicating that the photogenerated carrier generation and transport processes are largely preserved.

Similarly, the dark I–V characteristics exhibit only a slight change after 30 days. The small increase in dark current observed after storage may be attributed to minor interface relaxation, environmental adsorption effects, or subtle changes in the organic interfacial layer **[54]**. However, the magnitude of this variation remains limited and does not significantly affect the rectification behavior or device functionality. In the reverse bias region, the photocurrent measured after 30 days remains close to the initial value, confirming that the depletion region

and carrier separation efficiency are stable over time **[55]**. In the forward bias region, the nearly overlapping illuminated curves suggest that the barrier height and carrier injection characteristics undergo only negligible changes during storage. The minimal variation between the initial and aged measurements confirms the excellent environmental and operational stability of the Au/GA/p-Si/Al photodiode. The GA interfacial layer appears to provide effective passivation and interface protection, helping to maintain the electrical and optoelectronic characteristics of the device over extended periods. Overall, the results clearly demonstrate that the Au/GA/p-Si/Al photodiode exhibits good long-term stability, preserved UV photoresponse, and durable junction characteristics, making it a promising candidate for practical photodetector applications requiring reliable long-term operation.

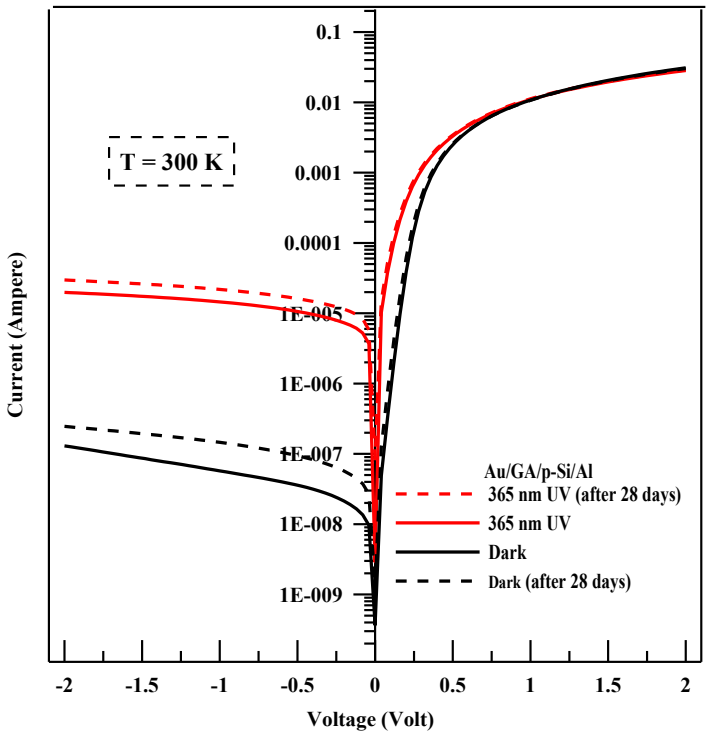


Fig. 16 Semi-logarithmic current–voltage (I–V) characteristics of the Au/GA/p-Si/Al photodiode measured under dark conditions and 365 nm UV illumination before and after 30 days of storage at 300 K.

Table 3 presents a comparative overview of the photodetection performance of the fabricated Au/GA/p-Si/Al photodiode with previously reported semiconductor-based photodiodes measured under an illumination intensity of 100 mW cm^{-2}. The comparison includes key parameters such as photosensitivity, photocurrent, responsivity, and specific detectivity, which are commonly used to evaluate photodiode efficiency and sensing capability. The proposed Au/GA/p-Si/Al device exhibits a photosensitivity of approximately 88, a photocurrent of 0.8×10^{-5} A, a responsivity of approximately 0.07 A W^{-1}, and a specific detectivity of about 2×10^{11} Jones. These values indicate that the fabricated device demonstrates a balanced combination of sensitivity, signal generation, and low-noise detection capability. When compared with other reported devices, the specific detectivity of the present photodiode is notably competitive. For instance, the obtained D^* value is significantly higher than those reported for $AgBiI_4$/n-Si

(3.74×10^{10} Jones), Al/3/p-Si (1.19×10^{10} Jones), Al/Cu_2CdSnS_4/pSi/Al (6.25×10^{9} Jones), and Au/PANI/p-Si/Al (6.21×10^{6} Jones). This comparison confirms that the insertion of the GA interfacial layer effectively improves the signal-to-noise characteristics of the Schottky junction. Although some devices such as Al/Y:ZnO/pSi/Ag (1.42×10^{12} Jones) and Ti/β-Ga_2O_3/Ni (2.33×10^{13} Jones) exhibit higher detectivity values, these systems are generally based on wide-bandgap oxide semiconductors specifically optimized for ultraviolet detection. In contrast, the Au/GA/p-Si/Al structure offers the advantage of a simpler fabrication route, low-cost p-Si substrate compatibility, and the beneficial interface engineering effect introduced by the GA organic layer.

The responsivity of the present device (~0.07 A W^{-1}) is moderate compared with some high-gain photodetectors; however, it remains superior to that of Au/PANI/p-Si/Al (2×10^{-6} A W^{-1}) and comparable to several organic/interfacial-layer-based photodiodes reported in the literature. Moreover, the measured photocurrent level of 0.8×10^{-5} A confirms efficient photocarrier generation and extraction under illumination. The photosensitivity value ($S\approx88$) is also appreciable and higher than several conventional metal/semiconductor devices, demonstrating the effectiveness of the GA layer in suppressing dark current while enhancing photocurrent generation. This improvement may be attributed to passivation of interface states, reduction of recombination centers, and modulation of the Schottky barrier height. Overall, the comparative data indicate that the fabricated Au/GA/p-Si/Al photodiode achieves a desirable balance between responsivity, photosensitivity, and detectivity. In particular, its detectivity in the order of 10^{11} Jones demonstrates excellent sensing capability, while the relatively simple device architecture and compatibility with silicon technology make it highly promising for practical photodetector and optoelectronic applications.

Table 3 Comparison of photodetector performance parameters

Device	P (mW/cm^{-2})	S	I_{ph} (A)	R (A/W)	D* (Jones)	Ref.
Au/GA/p-Si/Al (this work)	100	≈ 88	0.8 x 10^{-5}	≈ 0.07	≈ 2×10^{11}	(this work)
AgBiI4/n-Si device	100	59.14	5.95 x 10^{-4}	0.758	3.74 x 10^{10}	**[56]**
Al/3/p-Si	100	2.34	1.51 x 10^{-3}	1.927	1.19 x 10^{10}	**[57]**
Al/Y:ZnO/pSi/Ag	100	1674	-	0.12	1.42 x 10^{12}	**[58]**
Au/PANI/p-Si/Al	100	95	1.25 x 10^{-5}	2 x 10^{-6}	6.21 x 10^{6}	**[59]**
Al/Cu_2CdSnS_4/pSi/Al	100	-	-	45.32	6.25 x 10^{9}	**[60]**
Ag/Pd:Sn/ZnO/p-Si/Al	100	890	1.68 x 10^{-8}	0.25	4.25 x 10^{11}	**[61]**
Al/PyMIs/pSi/ Al	100	≈ 1000	-	≈ 4 x 10^{-4}	-	**[62]**
Au/PVA:Graphite-Er_2O_3/n-Si	100	1500	3.5 x 10^{-8}	≈1000	≈ 2×10^{10}	**[63]**
Ti/β-Ga_2O_3/Ni	100	-	2.17 x 10^{-8}	366.88	2.33 x 10^{13}	**[64]**

Conclusions

In this work, the influence of a GA (1,4-dimethyl-7-isopropylazulene) organic interfacial layer on the performance of a silicon-based Schottky photodiode was successfully demonstrated through the fabrication of an Au/GA/p-Si/Al device. The results clearly show that insertion of the GA layer significantly modifies the interfacial electronic properties and enhances the photodetection characteristics of the metal/semiconductor junction. Structural and morphological analyses confirmed the formation of a continuous GA thin film with nanostructured particle-like domains and partial short-range ordering. These features are expected to increase the effective interfacial area and influence carrier transport pathways. Optical investigations revealed that GA possesses strong ultraviolet absorption, a wide direct band gap (3.56 eV), and suitable electronic energy levels for charge-selective transport, indicating that the material can function efficiently as an interfacial modifier in optoelectronic devices.

Electrical characterization under illumination showed that the GA layer promotes illumination-induced barrier modulation and improved carrier extraction. The systematic decrease in barrier height together with the enhanced photocurrent response confirms that the interfacial GA layer facilitates photogenerated carrier separation and transport across the junction. The nearly linear dependence of photocurrent on illumination intensity further indicates stable and efficient photoresponse behavior. In addition, the device delivered competitive photodetection metrics, including detectivity in the order of 10^{11} Jones, reproducible ON/OFF switching, fast transient response (~0.1 s), and stable operation after long-term storage. The enhanced response under 365 nm illumination highlights the particular suitability of the device for ultraviolet sensing applications. Therefore, this study demonstrates that naturally derived azulene-based organic materials such as GA can serve as effective and low-cost interfacial layers for silicon photodiodes. Beyond the present device architecture, the proposed strategy may be extended to other semiconductor platforms for the development of high-performance, stable, and environmentally friendly next-generation photodetectors.

Funding Declaration
The authors received no financial support for the research, authorship, and/or publication of this article.

Conflict of Interest
The authors declare that they have no known financial interests, personal relationships, or competing interests that could have appeared to influence the work reported in this paper.

Data Availability Statement
The datasets generated and/or analyzed during the current study are available from the corresponding author on reasonable request.

References

[1] M. C. Bodur, S. Duman, I. Orak, S. Saritas, O. Baris, The photovoltaic and photodiode properties of Au/Carmine/*n*-Si/Ag diode, Optics & Laser Technology, 162 (2023), 109251; https://doi.org/10.1016/j.optlastec.2023.109251

[2] H. Seymen, Ş. Karataş, Investigation of electrical, photodiode and photovoltaic properties of Au/SiO_2/n-Si structures with GO and P_3C_4MT interface, Materials Chemistry and Physics, 310 (2023), 128449; https://doi.org/10.1016/j.matchemphys.2023.128449

[3] E. Gürgenç, A. Dıkıcı, F. Aslan, Investigation of structural, electrical and photoresponse properties of composite based Al/NiO:CdO/p-Si/Al photodiodes, Physica B: Physics of Condensed Matter, 639 (2022), 413981; https://doi.org/10.1016/j.physb.2022.413981

[4] S. Pujar, G. Rao K, Ni/ZnO Schottky photodiodes for high-performance ultraviolet detection: Influence of precursor molarity on structural and electrical properties, Optical Materials, 165 (2025), 117160; https://doi.org/10.1016/j.optmat.2025.117160

[5] Z. Yang, B. G. Kim, W. Jang, J. H. Park, D. H. Wang, High-performing acid-free PEDOT:PSS-based organic photodiodes for cardiovascular disease diagnosis, Advanced Functional Materials, 34(11) (2024), 2309271; https://doi.org/10.1002/adfm.202309271

[6] M**.** Erdoğan, Facile One-pot Synthesis of A Novel Propargyl-Azulene Hybrid Derivative: Cycloaddition Reaction and Some Spectroscopic Properties, Journal of the Institute of Science and Technology, 10(4) (2020), 2747-2758. https://doi.org/10.21597/jist.735838

[7] H. Kaçuş, A. R. Deniz, Z. Çaldıran, Ş. Aydoğan, A. Yeşildağ, D. Ekinci, The analysis of the current–voltage characteristics of the high barrier Au/Anthracene/n-Si MIS devices at low temperatures, Materials Chemistry and Physics, 143(2) (2014), 545-551; https://doi.org/10.1016/j.matchemphys.2013.09.030

[8] A. R. Deniz, The analyzing of I-V performance of PbO_2/n-Si heterojunction in the wide temperature range, Journal of Alloys and Compounds, 888 (2021), 161523; https://doi.org/10.1016/j.jallcom.2021.161523

[9] T. Kim, S. Lee, Y-W. Lee, D. Kim, Y. Yun, J-H. Bae, H. Lee, J. Park, Optimizing annealing temperature for enhanced electrical performance and stability of solution-processed In_2O_3 thin-film transistors, Micromachines, 16(10) (2025), 1091; https://doi.org/10.3390/mi16101091

[10] N. S. Gonçalves, J. A. Carvalho, Z. M. Lima, J. M. Sasaki, Size–strain study of NiO nanoparticles by X-ray powder diffraction line broadening, Materials Letters, 72 (2012), 36-38; https://doi.org/10.1016/j.matlet.2011.12.046

[11] E. Bastola, K. K. Subedi, K. Bhanderi, R. Ellingson, Solution-processed nanocrystal Based thin films as hole transport materials in cadmium telluride photovoltaics, MRS Advances, 3 (41) (2018), doi: 10.1557/adv.2018.349

[12] M. Marol, A. Garzon, J. Canales-Vazquez, J. C. Sancho-Garcia, Optoelectronic and semiconducting properties of conjugated polymers composed of Thiazolo[5,4-d]thiazole and arene imides linked by ethynylene bridges, The Journal of Physical Chemistry C, 120(43) (2016), 24583–24596; https://doi.org/10.1021/acs.jpcc.6b07240

[13] B. Salameh, A. M. Alsmadi, A. R. Hegazy, Optoelectronic properties and optical transitions in low concentrated aluminum-doped tin oxide thin films, Journal of Alloys and Compounds, 969 (2023), 172412; https://doi.org/10.1016/j.jallcom.2023.172412

[14] F. E. Cimilli Çatır, M. Sağlam, Annealing effect on I-V and C-V characteristics of Al/n-InP Schottky diodes at low temperatures, Materials Today: Proceedings, 46 (2021), 6979-6985; https://doi.org/10.1016/j.matpr.2021.03.275
[15] A. Fritah, L. Dehimi, F. Pezzimenti, A. Saadoune, B. Abay, Analysis of I–V–T characteristics of Au/n-InP Schottky barrier diodes with modeling of nanometer-sized patches at low temperature, Journal of Electronic Materials, 48(69) (2019), 3692-3698; https://doi.org/10.1007/s11664-019-07129-2
[16] Z. Çaldıran, A. R. Deniz, M. Sevim, Ş. Aydoğan, The heterojunction diode application of mesoporous graphitic carbon nitride (mpg-C_3N_4), Superlattices and Microstructures, 157 (2021), 106991; https://doi.org/10.1016/j.spmi.2021.106991
[17] A. Usha Rani, D. Surya Reddy, A. Ashok Kumar, V. Rajagopal Reddy, Structural, chemical, optical, electrical and photodiode properties of Au/ ZnPc/undoped-InP MPS-type diode using a ZnPc interlayer, Materials Science & Engineering B, 305 (2024), 117436; https://doi.org/10.1016/j.mseb.2024.117436
[18] T. Lazar, P. Gowrisankar, Study on structural, optical, and electrical properties of yttrium doped molybdenum oxide thin film and its MIS diode performance, Journal of the Indian Chemical Society, 101 (2024), 101216; https://doi.org/10.1016/j.jics.2024.101216
[19] M. C. Hacıismailoglu, M. Ahmetoglu, M. Haciismailoglu, M. Alper, T. Batmaz, Electrical and optical properties of Schottky diodes fabricated by electrodeposition of Ni films on n-GaAs, Sensors and Actuators A: Physical, 347 (2022), 113931; https://doi.org/10.1016/j.sna.2022.113931
[20] Ş. Uzun Çam, T. Serin, A. N. Yazıcı, Effect of Sn doping concentration on structural, optical and electrical properties of ZnS/p-Si (111) diodes fabricated by sol-gel dip-coating method, Materials Science in Semiconductor Processing, 127 (2021), 105693; https://doi.org/10.1016/j.mssp.2021.105693
[21] M. Sakthivel, S. Stella Mary, V. Balasubramani, Mohd Shkir, H. Elhosiny Ali, Enhanced electrical performance of Ag/Ba–Sn/n-Si/Ag hetero junction diode for photodiode applications, Physica B: Condensed Matter, 654 (2023), 414692; https://doi.org/10.1016/j.physb.2023.414692
[22] M. Ataei, M. R. Ferdavieslam, The Optimizing optical and electrical properties of Cu-doped MoO_3 thin films for photodiode applications, Optical Materials, 169 (2026), 117536; https://doi.org/10.1016/j.optmat.2025.117536
[23] A. Baltakesmez, S. Alptekin, Thermochromic 2D (n-BA)2NiI_xCl_{4-x} perovskite interlayer-integrated self-powered and reverse-biased Si-photodiode, Sensors and Actuators: A. Physical, 396 (2025), 117175; https://doi.org/10.1016/j.sna.2025.117175
[24] A. Demiroglu, M. Caglar, Investigation of physical and photodiode properties of Ir-doped NiO films, Physica B: Condensed Matter, 713 (2025), 417368; https://doi.org/10.1016/j.physb.2025.417368
[25] İ. Uzun, İ. Orak, Ö. Sevgili, M. Karakaplan, Investigation and comparison of various properties of diodes made using PTCDA and its synthesized ligand and brominated derivative, Materials Science & Engineering B, 317 (2025), 118147; https://doi.org/10.1016/j.mseb.2025.118147
[26] S. Duman, E. Yıldız Gül, M. Aydemir, H. Selvitopi, T. Öznülüer Özer, E. Tanrıverdi Eçik, Enhanced photodiode performance: Au/boron-dipyrromethene/n-Si/Ag structure unveiling

high photosensitivity and efficiency, Optics & Laser Technology, 181 (2025), 111648, https://doi.org/10.1016/j.optlastec.2024.111648
[27] V. Balasubramani, J. Chandrasekaran, V. Manikandan, T. Khac Le, R. Marnadu, P. Vivek, Upgraded photosensitivity under the influence of Yb doped on V_2O_5 thin films as an interfacial layer in MIS type Schottky barrier diode as photodiode application, Journal of Solid State Chemistry, 301 (2021), 122289; https://doi.org/10.1016/j.jssc.2021.122289
[28] K. U. Aiswarya, K. J. Arun, M. D. Aggarwal, Fabrication and characterisation of high response Cu/ (PVA-$CdWO_4$) / p-Si Schottky diode for Ultraviolet photo detection, Current Applied Physics, 80 (2025), 108-121; https://doi.org/10.1016/j.cap.2025.09.008
[29] A. Moumen, P. Rajabi Kalvani, F. Mattei, G. Foti, A. Parisini, R. Mosca, M. Pavesi, M. Bosi, L. Seravalli, F. Mezzadri, A. Baraldi, P. Mazzolini, S. Vantaggio, A. Bosio, R. Fornari, Self-powered NiO/κ-Ga_2O_3 heterojunction photodiode for fast broadband ultraviolet (UV) radiation detection, Optical Materials, 165 (2025), 117125; https://doi.org/10.1016/j.optmat.2025.117125
[30] A. Karabulut, D. E. Yıldız, M. Yıldırım, H. H. Güllü, A. Kocyigit, N. Tasaltın, A. Gulsaran, B. Bastug Azerj, M. Yavuz, The effects of Ppy-silicene composite on the performance of n-/p-type silicon semiconductor-based photodiodes, Sensors and Actuators: A. Physical, 379 (2024), 115996; https://doi.org/10.1016/j.sna.2024.115996
[31] B. Thakur, A. Mitra, R. Kumar, Self-powered $Ge_2Sb_2Te_5$ on n-Si photodiode for UV–Vis detection fabricated by Pulsed Laser Deposition, Optical Materials, 174 (2026), 117930; https://doi.org/10.1016/j.optmat.2026.117930
[32] S. Izmirli, S. Cavdar, Effect of film thickness on photodiode and photodetector performance of titanium dioxide (TiO_2) prepared via solution assisted spin coating method, Applied Surface Science, 688 (2025), 162187; https://doi.org/10.1016/j.apsusc.2024.162187
[33] H. K. Kaplan, High-speed Cu-doped ZnS/n-Si heterojunction photodiode for enhanced UV detection, Journal of Alloys and Compounds, 1038 (2025), 182849; https://doi.org/10.1016/j.jallcom.2025.182849
[34] S. Ruzgar, Y. Caglar, M. Caglar, The optoelectrical properties of rare earth element Eu doped Cu_xO based heterojunction photodiode, Chinese Journal of Physics, 72 (2021), 587-597; https://doi.org/10.1016/j.cjph.2021.05.017
[35] M. Erdoğan, A. R. Deniz, Z. Çaldıran, Exploring photodiode characteristics of a D-π-D type organic semiconductor incorporating a fluorenyl π-bridge and triphenylamine donors, Journal of Photochemistry & Photobiology, A: Chemistry, 469 (2025), 116532; https://doi.org/10.1016/j.jphotochem.2025.116532
[36] E. Daş, U. İncekara, Ş. Aydoğan, A comparative study on electrical characteristics of Ni/n-Si and Ni/p-Si Schottky diodes with Pinus Sylvestris Resin interfacial layer in dark and under illumination at room temperature, Optical Materials, 119 (2021), 111380; https://doi.org/10.1016/j.optmat.2021.111380
[37] A. A. Hendi, F. Yakuphanoglu, Graphene doped TiO_2/p-silicon heterojunction photodiode, Journal of Alloys and Compounds, 665 (2016), 418-427; http://dx.doi.org/10.1016/j.jallcom.2016.01.045
[38] G. Alan Sibu, V. Balasubramani, P. Gayathri, M. Aslam Manthrammel, Mohd Shkir, Manifesting the versatile properties of the Magnesium MOS diodes for optoelectronic

applications, Optical Materials, 164 (2025), 117047; https://doi.org/10.1016/j.optmat.2025.117047
[39] D. E. Yıldız, H. H. Gullu, M. Yıldırım, N. A. Morley, R. Sahingoz, Novel Al/CoFe/p-Si and Al/NiFe/p-Si MS-type photodiode for sensing, Nanotechnology, 36 (2025), 025203; https://doi.org/10.1088/1361-6528/ad857c
[40] A. Baltakesmez, D. Alp Baltakesmez, Investigation of interlayer role of SLp biomaterial synthesized by a sol-gel method for bioelectronic applications: hybrid photodiode, Journal of Sol-Gel Science and Technology, 116 (2025), 2064–2084; https://doi.org/10.1007/s10971-025-07012-z
[41] M. Jia, F. Wang, L. Tang, J. Xiang, K. S. Teng, S. P. Lau, High-performance deep ultraviolet photodetector based on NiO/β-Ga_2O_3 heterojunction, Nanoscale Research Letters, 15 (2020), 47; https://doi.org/10.1186/s11671-020-3271-9
[42] S. Koboyashi, Y. Anno, K. Takei, T. Arie, S. Akita, Photoresponse of graphene field-effect-transistor with n-type Si depletion layer gate, Scientific Reports, 8 (2018), 4811; doi:10.1038/s41598-018-22974-7
[43] C. Fan, Z. Liu, S. Yuan, X. Meng, X. An, Y. Jing, C. Sun, Y. Zhang, Z. Zhang, M. Wang, H. Zheng, E. Li, Enhanced photodetection performance of photodetectors based on indium-doped tin disulfide few layers, ACS Applied Materials & Interfaces, 13(30) (2021), 35889–35896; https://doi.org/10.1021/acsami.1c06305
[44] F. Suo, J. Tong, L, Qian, D. H. Zhang, Study of dark current in mid-infrared InAsSb-based hetero n-i-p photodiode, Journal of Physics D: Applied Physics, 51 (2018), 275102; https://doi.org/10.1088/1361-6463/aac8d0
[45] E. M. El-Menyawy, L. M. El-Khalawany, I. T. Zedan, Electrical conduction and photodiode properties of Au/Feq_3/p-Si/al hybrid heterostructure, Physica B: Condensed Matter, 685 (2024), 416067; https://doi.org/10.1016/j.physb.2024.416067
[46] A. Usha Rani, S. Ashajyothi, A. Ashok Kumar, V. Rajagopal Reddy, Exploration of photoresponsivity, specific detectivity and interface properties of Au/ZnPc/InP/In photodiode at different illumination wavelengths, Thin Solid Films, 809 (2025), 140594; https://doi.org/10.1016/j.tsf.2024.140594
[47] T. Lu, Y. Dai, T-Y. Lee, X. Zheng, G. Chen, Y. Su, Z. Chen, H-C. Guo, T. Wu, Advancing long-wavelength InGaN micro-LEDs as wavelength-selective detectors for white-light communication, ACS Photonics, 11(8) (2025), 3390–3400; https://doi.org/10.1021/acsphotonics.4c00861
[48] A. Gottwald, U. Kroth, E. Kalinina, V. Zabrodskii, Optical properties of a Cr/4H-SiC photodetector in the spectral range from ultraviolet to extreme ultraviolet, Applied Optics, 57(28) (2018), 8431-8436; https://doi.org/10.1364/AO.57.008431
[49] S. P. Sundarajan, N. K. Grady, N. Mirin, N. J. Halas, Nanoparticle-induced enhancement and suppression of photocurrent in a silicon photodiode, Nano Letters, 8(2) (2008), 624-630; https://doi.org/10.1021/nl073030+
[50] Z. Qiu, Z. Xu, W. Chen, X. Ma, Q. Qin, L. Wu, S. Wang, Q. Hang, L. Li, High-performance TiO_2 UV photodetectors with improved response time achieved through sol-gel synthesis and PDMS surface passivation, Optical Materials, 162 (2025), 116905; https://doi.org/10.1016/j.optmat.2025.116905

[51] M. Kumar, C. Y. Lee, H. Sekiguchi, H. Okada, A. Wakahara, Demonstration of a large-area AlGaN/GaN Schottky barrier photodetector on Si with high detection limit, Semiconductor Science and Technology, 28 (2013), 094005; doi10.1088/0268-1242/28/9/094005
[52] A. Hannaan, A. Rahman, A. Khandakar, P. Chelvanathan, B. Aissa, M. I. Hossain, Design and performance evaluation of an enhanced Ag_3CuS_2-based near-infrared photodetector for optoelectronic application, Next Materials, 9 (2025), 101266; https://doi.org/10.1016/j.nxmate.2025.101266
[53] A. Boutelala, F. Bourfa, M. Mahtali, Effect of light on electrical and photoelectrical characteristics of Al/TiO_2/p-Si Schottky diode, Journal of Materials Science: Materials in Electronics, 31 (2020), 11379-11389; https://doi.org/10.1007/s10854-020-03687-y
[54] C. Bi, S. V. Kershaw, A. L. Rogach, J. Tian, Improved stability and photodetector performance of $CsPbI_3$ perovskite quantum dots by ligand exchange with aminoethanethiol, Advanced Functional Materials, 29(29) (2019), 1902446; https://doi.org/10.1002/adfm.201902446
[55] X. Ma, R. A. J. Janssen, G. H. Gelinck, Trap-assisted charge generation and recombination in State-of-the-art organic photodetectors, Advanced Materials Technologies, 8(16) (2023), 2300234; https://doi.org/10.1002/admt.202300234
[56] E. Ünver, A. Toprak, A. A. Hussaini, M. Kuş, M. Yıldırım, Investigation and calculation of electrical performance of lead-free $AgBiI_4$ perovskite based Schottky photodiode using machine learning, Journal of Materials Science: Materials in Electronics, 36 (2025), 671, https://doi.org/10.1007/s10854-025-14728-9
[57] P. Karsili, A. Abourajab, M. Dinleyici, S. Altınışık, S. Koyuncu, G. Dolek, M. Kus, H. Icil, Aggregation− induced red− shift emission from self-assembled planar naphthalene diimide dye: Interlayer in a Schottky-type photodiode and DFT studies, Optical Materials, 155 (2024); 115902, https://doi.org/10.1016/j.optmat.2024.115902
[58] M. A. Siddiq, Synthesis of 2D yttrium zinc oxide nanosheets via simple chemical route toward high performance Schottky diode based on large charge carriers density and photoresponsivity, Materials Research Express, 11(5) (2024), 056304; https://doi.org/10.1088/2053-1591/ad4779
[59] A. R. Deniz, G. Gök, Enhanced photodiode performance of Au/PANI/p-Si diode: Characterization and analysis, Journal of Materials Research, 2026; doi: 10.1557/s43578-026-01818-5
[60] A. G. Al-Sehemi, A. Tataroğlu, A. Dere, A. Karabulut, A. A. Al-Ghamdi, F. Yakuphanoğlu, The structural, electrical, and photoelectrical properties of Al/Cu_2CdSnS_4 chalcogenide film/p-Si Schottky-type photodiode, 34(30) (2024); https://doi.org/10.1007/s10854-023-11465-9
[61] E. Elgazzar, Impact of Pd^{2+} and Sn^{4+} co-doping ZnO nanoflakes toward high-performing Schottky diode based on the generation of intermediate bands within the energy gap, Journal of Materials Science: Materials in Electronics, 35 (2024), 1697; https://doi.org/10.1007/s10854-024-13398-3
[62] A. O. Tezcan, P. Oruç, N. Tuğluoğlu, S. Eymur, Photosensitive properties of Schottky type photodiodes prepared by spin coating of isoniazid Schiff base thin film on p-Si, Optical and Quantum Electronics, 56 (2024), 989; https://doi.org/10.1007/s11082-024-06770-4

[63] F. Hanife, Y. Badali, Optical response of Au/n-Si schottky photodiode with an interface of graphite-Er_2O_3-doped polyvinyl alcohol (PVA) nanocomposite, Photonics and Nanostructures - Fundamentals and Applications, 66 (2025), 101446; https://doi.org/10.1016/j.photonics.2025.101446
[64] W-Y. Jiang, Z. Liu, Z-Y. Yan, C-L. Lu, P-G. Li, Y-F. Guo, W-H. Tang, High-performance dual-mode solar-blind sensor of a Si-doped β-Ga_2O_3 trench Schottky photodiode, IEEE Sensors Jornal, 21(17) (2021), 18663-18669; doi10.1109/JSEN.2021.3087715